

Wireless-Friendly Window Position Optimization for RIS-Aided Outdoor-to-Indoor Networks based on Multi-Modal Large Language Model

Jinbo Hou, Kehai Qiu, *Member, IEEE*, Zitian Zhang, Yong Yu, Kezhi Wang, *Senior Member, IEEE*, Stefano Capolongo, Jiliang Zhang, *Senior Member, IEEE*, Zeyang Li, Jie Zhang, *Senior Member, IEEE*

Abstract—This paper aims to simultaneously optimize indoor wireless and daylight performance by adjusting the positions of windows and the beam directions of window-deployed reconfigurable intelligent surfaces (RISs) for RIS-aided outdoor-to-indoor (O2I) networks utilizing large language models (LLM) as optimizers. Firstly, we illustrate the wireless and daylight system models of RIS-aided O2I networks and formulate a joint optimization problem to enhance both wireless traffic sum rate and daylight illumination performance. Then, we present a multi-modal LLM-based window optimization (LMWO) framework, accompanied by a prompt construction template to optimize the overall performance in a zero-shot fashion, functioning as both an architect and a wireless network planner. Finally, we analyze the optimization performance of the LMWO framework and the impact of the number of windows, room size, number of RIS units, and daylight factor. Numerical results demonstrate that our proposed LMWO framework can achieve outstanding optimization performance in terms of initial performance, convergence speed, final outcomes, and time complexity, compared with classic optimization methods. The building's wireless performance can be significantly enhanced while ensuring indoor daylight performance.

Index Terms—Building wireless performance, large language model, indoor daylight performance, reconfigurable intelligent surfaces, window design optimization, outdoor-to-indoor network.

I. INTRODUCTION

Jinbo Hou and Jie Zhang are with the Department of Electronic and Electrical Engineering, the University of Sheffield, Sheffield, UK (e-mail: jhou9@sheffield.ac.uk, jie.zhang@sheffield.ac.uk). Kehai Qiu is with the Department of Computer Science and Technology, University of Cambridge, Cambridge CB3 0FD, U.K. (e-mail: kq218@cam.ac.uk). Kehai Qiu is also with Brunel University London. Zitian Zhang is with the School of Information and Electronic Engineering, Zhejiang Gongshang University, Hangzhou, China (e-mail: zitian.zhang@mail.zjgsu.edu.cn). Yong Yu and Stefano Capolongo are with the Design & Health Lab, Department of Architecture, Built Environment and Construction Engineering, Politecnico di Milano, Italy (email: yong.yu@polimi.it, email: stefano.capolongo@polimi.it). Kezhi Wang is with the Department of Computer Science, Brunel University London, Uxbridge, Middlesex, UB8 3PH (email: kezhi.wang@brunel.ac.uk). Jiliang Zhang is with The State Key Laboratory of Synthetical Automation for Process Industries and The College of Information Science and Engineering, Northeastern University, Shenyang, China. (e-mail: zhangjiliang1@mail.neu.edu.cn). Zeyang Li is with the Centre for Wireless Innovation, Queen's University of Belfast, Belfast, BT3 9DT, UK (e-mail: lizeyang321@gmail.com).

Kehai Qiu, Kezhi Wang and Jie Zhang would like to acknowledge the partial support from the Eureka COMET / Innovate UK project (No: 10099265). Zeyang Li and Jie Zhang are the corresponding co-authors. Kezhi would like to acknowledge the support in part by the Royal Society Industry Fellowship (IF\R2\23200104)

IN 5G wireless communication systems, approximately 90% traffic occurs within buildings, posing unprecedented challenges to the design of indoor wireless networks. Moreover, building wireless performance (BWP) is greatly impacted and constrained by building characteristics such as windows, layouts, and materials as demonstrated in [1]. Therefore, the wireless performance of a building should be considered and optimized according to the demand of indoor communication networks during the building's design phase. This is particularly crucial for reconfigurable intelligent surfaces (RIS)-aided outdoor-to-indoor (O2I) communication networks, where indoor traffic demands are met by outdoor base stations (BSs) through intermediate transmissive reconfigurable intelligent surfaces (T-RISs) [2]. In such networks, walls and windows significantly impact the deployment strategy of T-RISs when mitigating the penetration loss and shadowing effects of buildings [3].

Currently, most researchers proposed deploying T-RISs on the walls of buildings [4]. The authors in [5] designed a dual-hop hybrid RIS-aided mmWave system featuring one passive and one active RIS on the surface of a building to maximize the signal-to-noise ratio of users by jointly optimizing the reflecting coefficients of the RISs and the beamforming vectors of the BSs. This optimization problem was divided into three sub-problems and solved using alternating optimization methods. The research in [6] proposed a policy gradient reinforcement learning method to jointly control the beamforming power of each user and the phase shifts of RISs to maximize spectral efficiency for both indoor and outdoor users in a wall-deployed simultaneously transmitting and reflecting (STAR)-RIS-assisted downlink communication system. Similarly, researchers in [7] addressed a wall-deployed STAR-RIS-aided three-dimensional indoor and outdoor localization problem by optimizing power allocation between refraction and reflection, as well as between two mobile stations, using a principal angle analysis method. Additionally, the research [8] investigated a wall-deployed hybrid double-RIS-aided and relay-aided system to eliminate the impact of building occlusion and penetration loss in O2I communication networks by proposing two closed-form algorithms for passive RIS beamforming.

Unfortunately, these wall-deployed T-RISs still experience significant penetration loss caused by concrete walls [9]. Moreover, wall-deployed RISs are difficult to reconfigure, replace, or repair due to high structural modification costs and the potential hazards associated with the rapid evolution of RIS-

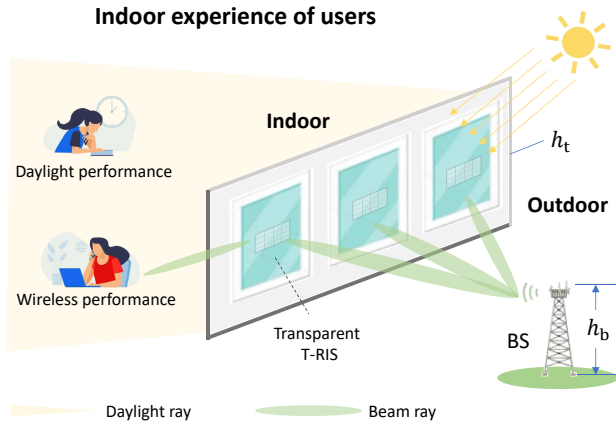


Fig. 1. Illustration of the indoor user's well-being experience considering the performance of wireless and daylight via transparent T-RISs.

related technologies [10]. Consequently, windows, as the most flexible components of a building, are promising to play a crucial role in RIS-aided O2I communication networks, as highlighted by recent research. Researchers in [11] proposed a window implementation strategy using a transparent metasurface lens, which facilitated installations on glass windows and other visually sensitive areas. This approach allowed the scattering characteristics of metasurfaces to be dynamically controlled, mitigating coverage holes in an O2I network while maintaining high optical transparency. Subsequently, a window-deployed active intelligent transmitting surface solution was proposed in [12] in an O2I network to optimize the indoor weighted traffic sum-rate. Additionally, window-deployed transparent active RISs were proposed in [13] for uplink enhancement in indoor-to-outdoor mmWave communication networks using closed-form optimization methods. These RISs can be integrated into optically transparent glass windows, providing environmental and aesthetic benefits without compromising visual effects.

However, these studies have primarily focused on the deployment of RISs while neglecting the impact of window attributes, particularly the positioning of windows. Inadequate window placement can result in the suboptimal placement of T-RISs, leading to a deterioration in indoor wireless communication performance, which subsequently affects the quality of experience (QoE) of indoor users. Meanwhile, the window placement is also crucial for indoor daylight performance [14], which significantly influences indoor users' QoE in terms of their mood, morale, mental state, and health [15].

Therefore, in this paper, we first investigate a passive T-RIS-aided O2I network with indoor blockages and aim to optimize both indoor wireless and daylight performance simultaneously by adjusting the positions of windows to enhance the overall QoE of indoor users as shown in Fig. 1. We then formulate a joint optimization problem that addresses indoor wireless performance and daylight performance subject to constraints on the minimum interval of windows and minimum indoor daylight requirements. To tackle this problem, we design a large language model (LLM)-based window optimization (LMWO) framework, followed by specific simulations and discussions. Our contributions can be summarized as follows:

- To our best knowledge, this is the first work to concurrently optimize the performance of the wireless network and daylight system in a passive T-RIS-aided O2I network with a specific focus on the role of windows in enhancing the well-being QoE of indoor users through a problem formulation.

- Secondly, we propose a novel LLM-based optimization framework to address this challenge by leveraging the pre-training knowledge, human-like learning capacity, and strong generalization ability of LLMs. Within this framework, an initialization module and an optimization module are designed to iteratively improve the performance of the LLM-based optimizer by interacting with the target environment.

- Thirdly, we design a prompt template for the LLM-based optimizer that incorporates five categories of information to ensure the effective embedding of redundant information with standardized formats. Additionally, we construct environmental feedback as a fusion of multi-modal data (e.g. text and image) to enhance the generated solutions of LLMs through cross-verification of diverse data types.

- Finally, simulation results demonstrate that our proposed LMWO framework significantly outperforms the classic heuristic algorithm, simulated annealing genetic algorithm (SAGA) in terms of initial performance, convergence speed, time complexity, and final performance. Additionally, we investigate the impact of the number of windows, number of RIS units, room size, and daylight factor on the performance of the LMWO framework.

The rest of this paper is structured as follows: Section II discusses the system models for both the wireless system and daylight system with a joint optimization problem formulation. Section III details the basic knowledge of LLMs and our proposed LMWO framework. Section IV introduces the baseline algorithm SAGA. Section V includes an experimental setting and a discussion of the results with an analysis of influence elements. Finally, we conclude our work and present potential future directions in section VI.

II. SYSTEM MODEL AND PROBLEM FORMULATION

In this section, we introduce the wireless network model of a passive T-RIS-aided O2I network, followed by a daylight evaluation system for the indoor scenario. Combining these two systems, a joint optimization problem is formulated considering both wireless traffic sum rate and daylight illumination performance.

A. Wireless Network Model

The wireless network model of a typical passive T-RIS-aided O2I network is built on our previous research [16] as shown in Fig. 2. The focused rectangular workplace room has width W_r , length L_r , altitude height H_r , and N windows on its long side wall of the near end. All windows have a consistent size of L length and W width. In particular, U passive T-RIS units are uniformly deployed on the centre of windows with a fixed beam orientation to enhance the wireless communication between an outdoor BS with N_t antennas and an indoor user with a single antenna. We assume that the

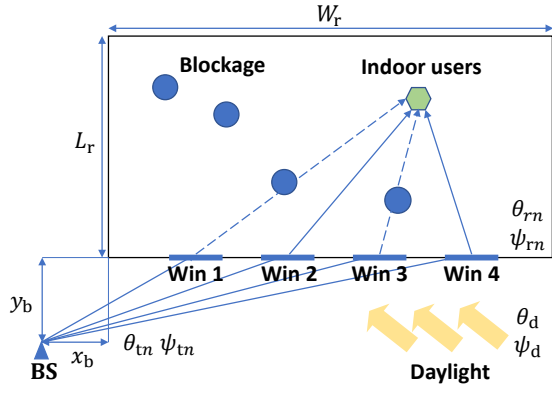


Fig. 2. The wireless network and daylight system, where θ and ψ represent the elevation and azimuth angle of corresponding links, respectively, and "Win" is an abbreviation for "window".

transmission from the BS to each RIS of windows is non-blocked and the direct transmission between the BS and UE is not considered due to the huge penetration loss. Specifically, the BS is H_t altitude height and located at $(0,0)$ in a 2-dimension Cartesian coordinate system. The left near point of the building is located at (x_b, y_b) . The central positions of windows are presented as $\mathcal{P} = \{(x_1, y_b), (x_2, y_b), \dots, (x_N, y_b)\}$. The beam elevation angles and azimuth angle of window-deployed RISs are denoted as $\Theta_r = \{\theta_{r1}, \theta_{r2}, \dots, \theta_{rN}\}$ and $\Psi_r = \{\psi_{r1}, \psi_{r2}, \dots, \psi_{rN}\}$, respectively.

Inside the room are M uniform measurement points to assess indoor wireless performance. For each measurement point, there is a user weight value to present the probability of the user appearing at this point following the function of the 2-dimensional joint beta distribution, which can represent the probability of traffic demand requirements and is presented as $\mathcal{W} = \{w_1, w_2, \dots, w_M\}$. Meanwhile, indoor environmental elements like furniture, pillars, and decorations are considered to be blockages which are modelled as cylinders with an average radius of R . The distribution of the blockages' centres follows the Poisson point process (PPP) with a density ρ . Considering the high penetration loss of indoor blockages, only line-of-sight (LoS) transmission is considered [3], [17]. Thus, according to the propagation model in [18], the average received power of the signal transmitted by the T-RIS on the n th window is shown as Eq. (1).

$$P_n = \frac{P_t N_t^2 d_x^2 d_y^2 \lambda^2 \cos \theta_{tn} \omega^2 (\sum_{i=1}^{\sqrt{U}} \sum_{j=1}^{\sqrt{U}} \exp(-j \phi_{n,i,j}))^2}{16\pi^2 d_{n1}^2 d_{n2}^2}, \quad (1)$$

where P_t is the transmit power of the signal from the BS, $d_x \times d_y$ is the size of the units of passive T-RISs on the n th window, λ is the wavelength of the carrier signal, ω is the penetration loss when the signal passes through the window, d_{n1} is the distance between the n th window and the BS, d_{n2} is the distance between the n th window and the user, respectively, $\phi_{n,i,j}$ is the phase of the wave reflected by the i th row and j th column unite on the RIS of the n th window and can be calculated as:

$$\phi_{n,i,j} = \phi_{a,n,i,j} - \phi_{r,n,i,j}, \quad (2)$$

where $\phi_{a,n,i,j}$ is the phase shift of the wave due to the location of the i th row and j th column unite on the RIS of the n th window as shown in Eq. (3), $\phi_{r,n,i,j}$ is the field pattern of the i th row and j th column unite on the RIS of the n th window as shown in Eq. (4). θ_{tn} and ψ_{tn} are the elevation and azimuth angle from the BS antennas to the centre of the RIS of the n th window, θ_{rn} and ψ_{rn} are the elevation and azimuth angle from the centre of the RIS of the n th window to the UE, θ'_{rn} and ψ'_{rn} are the desired elevation and azimuth angle from the centre of the RIS of the n th window to the UE.

Subsequently, the received traffic data rate of the measurement point m is derived by:

$$\gamma_m = \sum_{z \in \mathcal{Z}} P_{\text{LoS}}(z) B \log \left(1 + \frac{(\sum_{n \in z} \sqrt{P_n})^2}{\sigma_m^2} \right), \quad (5)$$

where z is the set of unblocked RISs, \mathcal{Z} is the possible combinations of RISs, e.g. $\{(1, 2, 3), (1, 2), (1, 3), (1), (2), (3)\}$ when there are three window-deployed RISs, $P_{\text{LoS}}(z)$ is the probability that the RISs from the set z is unblocked as the derivation Eq. (14) and Eq. (20) in [16], B is the channel bandwidth, σ_m^2 is the power of the additive white Gaussian noise (AWGN) at measurement point m .

B. Daylight Evaluation Model

For the indoor daylight analysis, daylight performance is evaluated using ray-tracing algorithms implemented through the Radiance and Daysim plugins within the Rhinoceros 3D Grasshopper software environment [19]. The ray-tracing method offers the most accurate and detailed results [15], considering the diverse daylight sources, the diffuse reflection phenomena, and the complexity of light propagation paths. Specifically, Radiance is a lighting simulation tool based on hybrid deterministic-stochastic ray tracing approaches [20] developed by Greg Ward Larson at Lawrence Berkeley National Laboratory. Radiance provides a realistic representation of light interactions by incorporating weather and illumination data into the indoor simulation model in compliance with EU Building Design standards [21]. Subsequently, Daysim analyses daylight performance using algorithms from Radiance. Additionally, natural weather and illumination data are introduced from the Ladybug [22], an open-source project focused on environmental design.

Inside the room, M measurement points are established to assess daylight, consistent with the wireless network model. For each measurement point, a single-day grid analysis is conducted on the winter solstice (the 21st of Dec.) at 15:00, considering only external natural and sunlight. the elevation and azimuth angles from the sunlight source to the centres of windows are denoted by θ_d and ψ_d , respectively. The daylight transmission rate of the windows used is presented as β using double-layer soda-lime glass. In terms of light reflection, the simulation calculates two bounces off the wall, floor, and ceiling surfaces with reflection coefficients, represented by F_w , F_f , and F_c , respectively. The illumination degree I_m at the m th measurement point (lux as unite) is calculated as:

$$I_m = I_m^1 + \widetilde{I}_m^1 + I_m^s + \widetilde{I}_m^s, \quad (6)$$

where I_m^l and \widetilde{I}_m^l are the direct and indirect illumination from the skylight, respectively, I_m^s and \widetilde{I}_m^s are the direct and indirect illumination from solar radiation, respectively. In particular, the direct ones include the direct light and solar illumination transmitted through windows. The indirect ones include the inter-reflected light, both internal and external reflections. Consequently, the output set of daylight illumination levels for all measurement points is presented as $\mathcal{I} = \{I_1, I_2, \dots, I_M\}$.

C. Problem Formulation

To improve the overall QoE of indoor users, wireless performance and daylight performance are simultaneously optimized by adjusting the window positions and beam directions of window-deployed RISs according to an indoor user weight matrix \mathcal{W} . The optimization results are compared against those of the common uniform-distributed window (UDW) strategy, where windows are uniformly implemented with beam directions perpendicular to the surface. The improvement of wireless performance ϕ_w is calculated as:

$$\phi_w = \frac{\sum_{m=0}^M \gamma_m / \gamma'_m \cdot w_m}{M}, \quad (7)$$

where γ'_m presents the received traffic data rate at the m th measurement point in UDW strategy. Similarly, the improvement of daylight performance ϕ_d is calculated as:

$$\phi_d = \frac{\sum_{m=0}^M I_m / I'_m \cdot w_m}{M}, \quad (8)$$

where I'_m presents the daylight illumination degree at the m th measurement point in UDW strategy. Finally, the optimization problem is formulated as:

$$\begin{aligned} \phi_o &= \max_{\mathcal{P}, \Theta_r, \Psi_r} (\phi_w + \eta \cdot \phi_d), \\ \text{s.t. } \phi_d &\geq \mathcal{T}_{\min}, \\ x_{n+1} - x_n &\geq d_{\min}, \forall x_n \in \mathcal{P}, \end{aligned} \quad (9)$$

where ϕ_o is the overall QoE optimization performance, η is adopted as daylight factor to control the optimization tendency, where higher values indicate a greater focus on sunlight, \mathcal{T}_{\min} is the minimum daylight improvement requirement to guarantee indoor daylight performance, d_{\min} presents the minimum distance between centres of windows, which is larger than the window width for aesthetic considerations.

This optimization problem is a non-convex problem caused by the following factors: i. the complexity and non-convexity caused by the blockage distribution and user distribution; ii. the sophisticated nature of the realistic ray tracing model employed for the daylight evaluation system; and iii. the

constraints imposed by variables and systems. To address these challenges, we propose an LLM-based optimization framework, leveraging the pre-trained knowledge and continuous learning capacity of LLMs.

III. METHODOLOGY

In this section, we first introduce the foundation of LLMs as optimizers as depicted in Fig. 3, accompanied by a concise literature review of their current applications. Then, we present the design of the LLM prompt template and multi-modal feedback for our focused optimization problem, followed by a specific demonstration of the LMWO framework.

A. LLM as Optimizer

Recently, LLMs have garnered tremendous attention and are famous for ChatGPT, enabled by transformer technology [23]. LLMs are distinguished by their ability to generate human-like contextually appropriate and grammatically correct outputs due to their extensive parameters, trained on vast text datasets covering diverse domains of human life [24]. Consequently, it is plausible that LLMs contain human-like capacities of continuous learning through trial and error and exhibit reasonable decision-making abilities, making them potential ideal optimizers for various optimization problems across different domains.

However, the application of LLMs as optimizers is significantly limited by issues such as hallucinations answers (e.g. incorrect and nonsensical content), knowledge out-of-date, and limited mathematical capacities [25]. To address these limitations, a robust framework and proper prompt design [26] is necessary to activate the optimization capabilities of LLMs, ensuring accurate, knowledge-aligned, and condition-compliant output. Specifically, prompts, which are text strings designed for interaction with LLMs, allow LLMs to integrate user-defined parameters of target systems, provide essential information on optimization problems, leverage professional simulation results from external tools (e.g. Python, Matlab, and Ranplan [27]), and incorporate expert human knowledge.

Currently, LLM-related optimization methods have shown impressive optimization capabilities across various research domains, including essay writing, code explanation, debugging, education, customer service, content creation, and healthcare [28]–[31]. In the wireless communication field, LLM-related research is advancing rapidly. The authors in [32] proposed a comprehensive WirelessLLM framework for adapting and enhancing LLMs to address wireless communication networks' unique challenges and requirements. A pre-trained LLM-empowered framework was proposed in [33] to perform

$$\phi_{a,n,i,j} = \text{mod}\left(-\frac{2\pi}{\lambda}(\sin \theta_{tn} \cos \psi_{tn} + \sin \theta_{rn} \cos \psi_{rn})(m - \frac{1}{2})d_x + (\sin \theta_{tn} \sin \psi_{tn} + \sin \theta_{rn} \sin \psi_{rn})(n - \frac{1}{2})d_y, 2\pi\right). \quad (3)$$

$$\phi_{r,n,i,j} = \text{mod}\left(-\frac{2\pi}{\lambda}(\sin \theta_{tn} \cos \psi_{tn} + \sin \theta'_{rn} \cos \psi'_{rn})(m - \frac{1}{2})d_x + (\sin \theta_{tn} \sin \psi_{tn} + \sin \theta'_{rn} \sin \psi'_{rn})(n - \frac{1}{2})d_y, 2\pi\right). \quad (4)$$

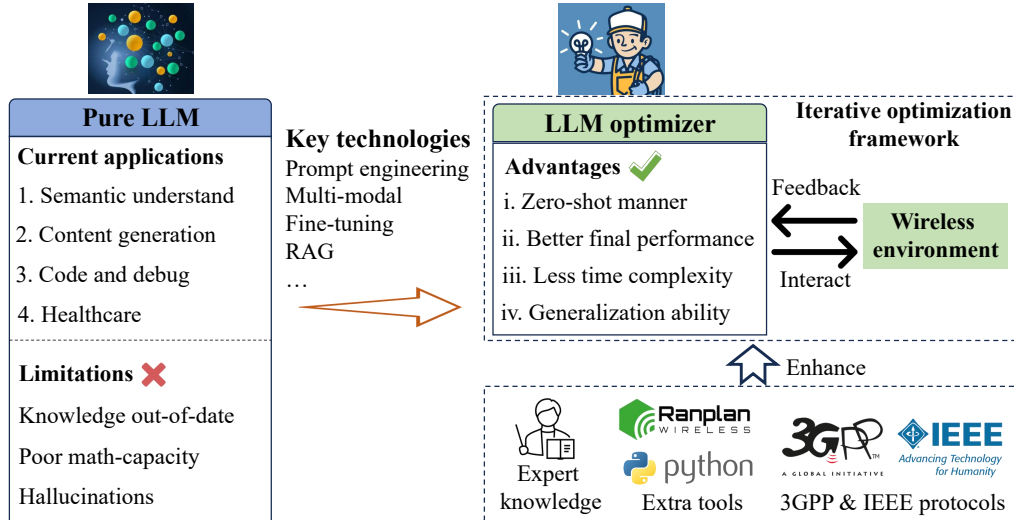


Fig. 3. The overview of LLM-based optimizers.

fully automatic network intrusion detection with three in-context learning methods to enhance the performance of LLMs without further training. The authors in [34] proposed a workflow for automated network experimentation relying on the synergy of LLMs and model-driven engineering, where the experiment code was generated based on the textual description. The research in [35] presented autonomous edge AI systems to organize, adapt, and optimize themselves, leveraging the power of LLMs to meet users' diverse requirements and generating a privacy-preserving manner code to train new models. In [36], the authors introduced an LLM-based optimizer for wireless network planning and optimization, focusing on optimizing the number and placement of wireless access points. Moreover, the research in [37] leveraged the analytical capabilities of LLMs, combined with key data to optimize RIS-based communication systems and achieve energy-efficient performance in real-time.

In summary, unlike conventional optimization approaches that require step-by-step programming, LLM-based optimizers do not require detailed and precise optimization execution steps when interacting with environments and receiving feedback. Moreover, LLM-based optimizers offer potentially effective solutions for complex optimization problems thanks to their extensive pre-trained data, unique multi-modal understanding mechanisms, and continuous learning capabilities. According to [29], [38], we summarize four prime advantages of LLM-based optimizers: i. zero-shot capability [39] and warm start performance; ii. improved final performance; iii. reduced time and faster convergence; and iv. model-free nature and generalization ability, which align well with the requirements of our focused optimization problem.

B. LMWO Framework

The following introduces the workflow of the LMWO framework including its inputs, outputs, core modules, and prompts designed for optimizing wireless and daylight performance as depicted in Fig. 4 (a). In this framework, prompt engineering serves as the primary approach for instructing

the LLM and integrating LLM with the target environment, enabling an iterative optimization framework.

Specifically, the workflow begins with a user distribution matrix from the target room as the input. Then, an initialization module is designed to generate a qualified initialization. Subsequently, an optimization module refines the solution iteratively until stability. Finally, the solution with the best optimization result is output as the final solution. In these modules, three reproducible prompts are constructed to provide task-oriented instructions, strictly define the format, and embed environmental feedback to LLMs as instructions for the target optimization problem as shown in Fig. 4 (b). To supply LLMs with redundant information, we propose a standardized prompt template that includes five categories of information and organizes reproducible, structured prompts [31], including task description, environmental information, input & output formats, historical experience, and expert knowledge. This approach ensures that comprehensive contextual information enables LLMs to better understand the optimization problem and provides sufficient cues for accurate inference. Consequently, LLMs can generate accurate outputs while minimizing hallucination effects.

Moreover, we design the wireless environment feedback as a fusion of multi-modal information [40], containing wireless sum rate performance ϕ_w , daylight illumination performance ϕ_d , a heatmap figure of wireless sum rate performance at measurement points, and a heatmap figure of daylight illumination performance at measurement points as shown in Fig. 4 (c). By capturing different types of environmental feedback (e.g., text and images), LLMs can establish connections between feedback data and enhance situational awareness through cross-verified information. Therefore, LLMs can provide more reasonable solutions for our optimization problems. Next, we discuss the details of two core modules:

1) *Initialization module:* The initialization module determines the window positions \mathcal{P} and the RIS beam directions Θ_r and Ψ_r through an LLM-based initializer and interactions with the wireless network and daylight evaluation system.

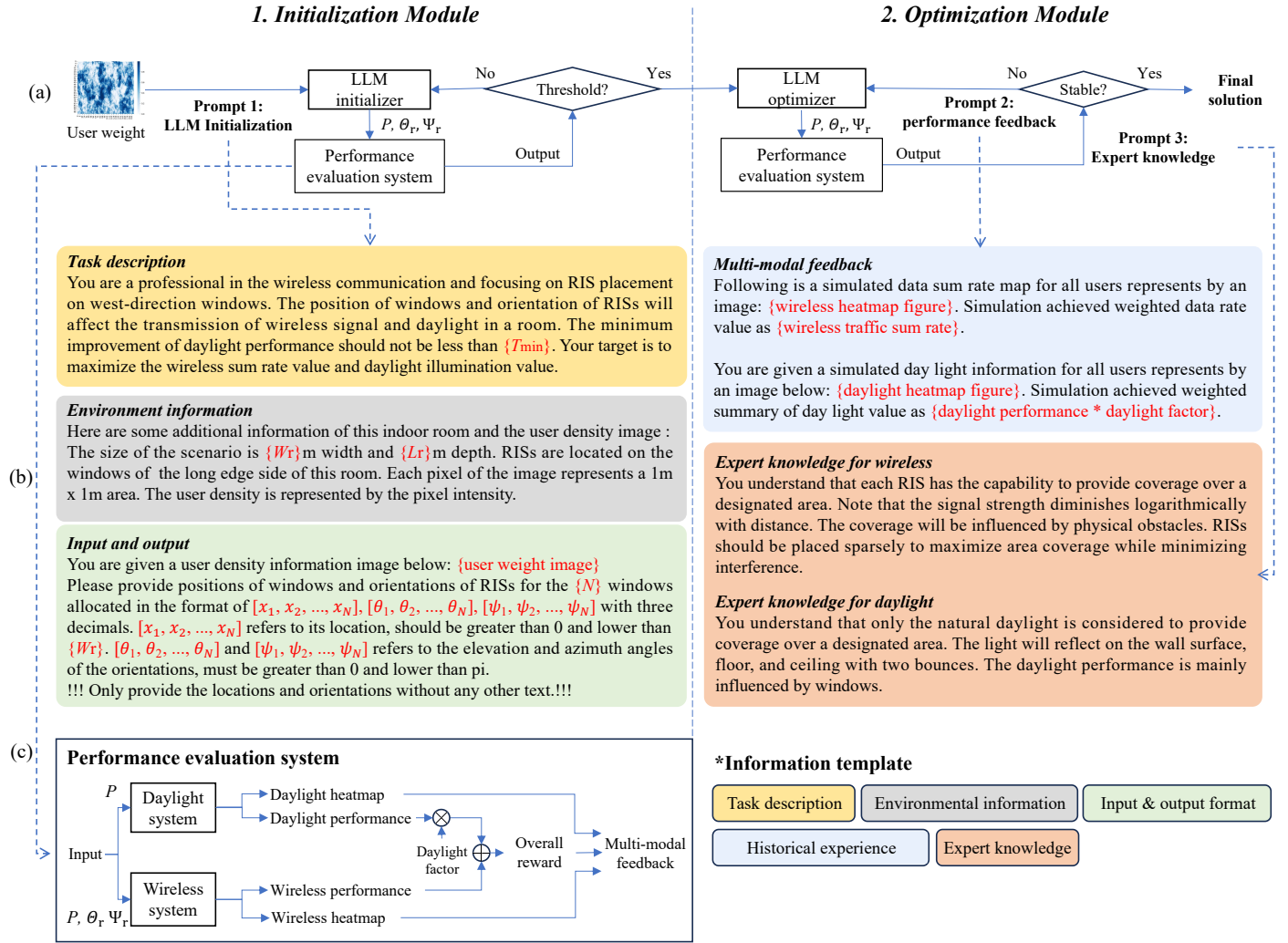


Fig. 4. The structure of the LMWO framework, including two modules, three prompts, information template, and the performance evaluation system.

Algorithm 1 : Initialization module

- 1: input the **initialization prompt 1** to the LLM;
- 2: achieve \mathcal{P} , Θ_r , and Ψ_r from the LLM.
- 3: interact with the wireless and daylight evaluation systems to get the multi-modal output;
- 4: **if** reward $\leq \mathcal{T}_i$ **then**
- 5: go back to step 2;
- 6: **end if**
- 7: forward the initialization to the optimization module;

This process involves iterations to achieve qualified results that exceed threshold \mathcal{T}_i , emphasizing the significance of initial performance for the LMWO framework as illustrated in Algorithm 1. Within this module:

- **LLM initialization prompt** is constructed by the information of task description, environmental information, input format, and output format as shown in Fig. 4 (b). This information provides details about the optimization task (e.g. variables, optimization goals, and constraints), environmental information of the target room, and suffi-

Algorithm 2 : Optimization module

- 1: achieve the initialization solution;
- 2: interact with the wireless system and the daylight evaluation system;
- 3: **if** stable or maximum steps **then**
- 4: end the process and output the final solution;
- 5: **else**
- 6: construct the **performance feedback prompt** by leveraging the multi-modal output and the **expert knowledge prompt**.
- 7: achieve \mathcal{P} , Θ_r , and Ψ_r from the LLM.
- 8: go back to step 2;
- 9: **end if**

cient instructions for the input and output with restricted format and appropriate guidance.

2) *Optimization module*: Subsequently, the optimization module contains a combinatorial LLM-based optimizer that iteratively updates performance based on the results from the initialization module as shown in Algorithm 2. In each itera-

tion, window positions and RIS beam directions are generated and forwarded to the corresponding wireless and daylight evaluation system. This process continues until a stable status or maximum iteration steps. Within the optimization module, there are two types of prompts:

- **Performance feedback prompt** informs the LLM about the feedback information from the wireless and daylight system model using the historical experience information as shown in Fig. 4 (b) to iteratively adjust and improve the LLM's response based on the feedback.
- **Expert knowledge prompt** uses the expert knowledge information as shown in Fig. 4 (b) to integrate additional indoor wireless network knowledge and indoor daylight design knowledge from physical, mathematical, and experiential aspects into the LLM and enhance its decision-making capability. Incorporating expert knowledge equips the LLM with an enhanced capacity in wireless communication and architectural domains to address complex optimization problems.

IV. THE SAGA ALGORITHM

We introduce the heuristic algorithm SAGA as a benchmark, which combines the genetic algorithm (GA) and simulated annealing algorithm (SA) [41]. GA is an iterative optimization algorithm with a computational mechanism inspired by the Darwin theory of evolution [42]. In the natural environment, well-fitness individuals are likely to generate new individuals by crossover and mutation processes of chromosomes to inherit genes. Accordingly, GA encodes a potential solution as a chromosome and variables of this solution as genes for an optimization problem. Here, we formulate populations, individuals, chromosomes, and generation processes according to the optimization problem of this paper. Assuming K individuals constitute a population, represented by $\mathcal{A} = \{A_1, A_2, \dots, A_K\}$. The chromosome of the k th individual A_k refers to the set of positions of windows and directions of window-deployed RISs, denoted as $\{x_1, x_2, \dots, x_N, \theta_{r1}, \theta_{r2}, \dots, \theta_{rN}, \psi_{r1}, \psi_{r2}, \dots, \psi_{rN}\}$ with a fitness value $f(A_k)$, which is defined as the overall performance of target environment.

In each generation process, parents individuals are randomly selected among the population to generate offspring chromosomes by conducting crossover and mutation processes after random initialization of the population. In the crossover process, parents' chromosomes partially exchange on the gene points with a probability of P_c , allowing offspring to inherit genes from their parents and increasing solution diversity. Next, the mutation process is utilized as an exploration mechanism to randomly modify certain gene positions on an individual's chromosome with a probability of P_m , increasing the diversity of the population and preventing the algorithm from getting stuck in local optima. Finally, weaker solutions are removed and replaced by better solutions according to their fitness. Additionally, an elitism principle is leveraged to maintain the best individuals of the existing \mathcal{E} generation after crossover or mutation to provide exploration guidelines.

However, GA is always trapped in the local optimal solution with low-speed convergence without sufficient exploration

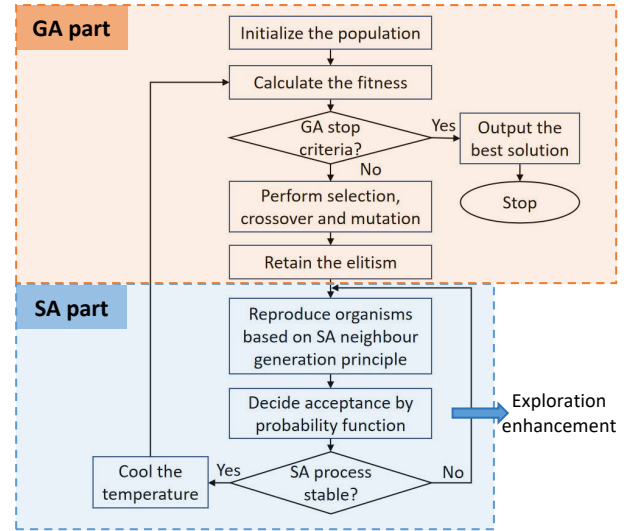


Fig. 5. The flowchart of the SAGA algorithm.

mechanisms. Therefore, we combine the SA part to provide the search advance. SA is a heuristic optimization algorithm inspired by the physical annealing process with a temperature mechanism to probably accept worse performance solutions. In each iteration, the temperature starts from high temperature T_{\max} and gradually cools down to low temperature T_{\min} . At high temperatures, a worse-performance solution is more likely to be accepted. While at low temperatures, a worse-performance solution is more probable to be inclined. The criterion of acceptance is according to the Metropolis criterion as shown in Eq. (10) and Eq. (11), where $\Delta E = f(A_{\text{new}}) - f(A_k)$, μ presents the cooling factor of temperature.

$$P = \begin{cases} 1, & f(A_{\text{new}}) < f(A_k), \\ e^{-\Delta E/T_t}, & \text{otherwise.} \end{cases} \quad (10)$$

$$T_t = \begin{cases} \frac{f(A_k)}{\log 5}, & t = 1, \\ \mu T_{t-1}, & t > 1. \end{cases} \quad (11)$$

Detailed operation procedure of the SAGA algorithm is shown in Fig. 5 as described in Algorithm 3.

V. SIMULATION RESULT AND DISCUSSION

In this section, we first introduce the simulation settings employed in this paper. Then, we present the experimental results of the LMWO framework compared with two benchmark methods. Finally, we discuss the influence of the number of windows, daylight factor, number of RIS units, and room size on the performance of the LMWO framework, followed by a time complexity analysis.

A. Simulation Setting

In this simulation, the room is assumed to be located in Sheffield the UK, with west-facing windows. The meteorological data of Sheffield is sourced from EnergyPlus Weather (EPW) files downloaded from the website [22]. Moreover, we consider two rectangular room size scenarios: **Room 1** with

Algorithm 3 : SAGA algorithm

- 1: Initialize parameters of SAGA: initial temperature T_{\max} , the lowest temperature T_{\min} , and cooling factor μ . Randomly initialize population \mathcal{A} with K individuals.
- 2: Evaluate the fitness of each individual in \mathcal{A} by interacting with the environment.
- 3: **while** GA process unstable and step \leq max step **do**
- 4: Perform the process of generating a new solution by applying selection, crossover, and mutation processes to create offspring populations \mathcal{O} .
- 5: Retain \mathcal{E} best fitness individuals from the old generation as elites.
- 6: **while** the SA process unstable and $T > T_{\min}$ **do**
- 7: Reproduce the individual with a minor deviation based on the neighbour function and evaluate the fitness of each individual in \mathcal{O} by interacting with the environment.
- 8: **for** each individual in \mathcal{O} **do**
- 9: Decide whether to accept the new individual according to the probability function and Metropolis criterion as shown in Eq. (10) and Eq. (11).
- 10: **end for**
- 11: **end while**
- 12: Update the temperature with $T = T * \mu$.
- 13: **end while**
- 14: Output the best fitness individual as the final solution.

10m width and 10m length and **Room 2** with 10m width and 20m length. In each scenario, the random choice (RC) method and SAGA algorithm are employed as the baseline algorithms. In the RC method, all variables are randomly chosen within their respective constraints. The maximum operation steps of SAGA and RC methods are set to 1500, which is sufficient to achieve stable convergence. Towards the LMWO framework, if the result does not change in five steps or reaches a maximum of ten steps, the optimization process will stop. Additionally, each method is conducted ten times to obtain an averaged result to mitigate individual randomness. The detailed parameters are shown in Table I.

Our simulations are executed using the Anaconda 3 software environment with Python 3.12.4 on a computer with a 2 Core Intel i5-10505 3.20GHz CPU and 16 GB RAM. For the daylight evaluation system, the Radiance 5.2.d and Daysim 4.0 software are adopted within Rhinoceros 8 SR7. Additionally, the LLM component utilizes the Anthropic LLM via its commercial API [43].

B. Performance of LMWO Framework

In this subsection, we present the simulation results of the average optimization performance of the LMWO framework versus the iteration steps compared with SAGA and RC methods. Fig. 6 depicts the average performance of the LMWO framework in Room 1 with two, three, and four windows, respectively. In all three subfigures, the LMWO framework consistently exhibits outstanding performance in the aspects of warm start, faster convergence, and higher final performance,

TABLE I
SIMULATION PARAMETERS

Parameter	Value	Parameter	Value	Parameter	Value
λ	0.01 m	ω	5 dB	N_t	32
L_r	20 m	W_r	10 m	P_t	1 W
x_b	20 m	y_b	30 m	h_b	30 m
L	1.2 m	W	0.9 m	h_t	10 m
R	0.2 m	G	8	ρ	0.01 m^{-2}
d_x	0.005 m	d_y	0.005 m	U	900
T_{\max}	100	T_{\min}	5	μ	0.98
P_m	0.3	P_c	0.9	\mathcal{E}	2
F_w	0.6	F_f	0.4	F_c	0.7
η	5	ϕ_d	220°	θ_d	86°
d_{\min}	0.9 m	\mathcal{T}_{\min}	0.8	\mathcal{T}_i	5

significantly surpassing the other methods. For instance, in the four-window scenario, the LMWO method starts from 8.5 and reaches a stable convergence in 10 iteration steps, achieving a final performance of 15.2. In contrast, the performance of the SAGA method starts from 6 and then stabilizes after 600 iterations with a final performance of approximately 13. Additionally, the RC method performs even worse, starting from 3 and reaching a final performance of 10.3. Compared with the SAGA method, the LMWO framework method achieves enhancements of 41.7% and 16.9% in the start performance and final performance, respectively with a much faster convergence speed.

Similarly, the average optimization performance of the LMWO framework in Room 2 is remarkable as shown in Fig. 7, which depicts the average optimization performance of our LMWO framework versus the iteration steps. For example, in the four-window scenario shown in Fig. 7 (c), the LMWO framework presents notable optimization performance with a 6.55 start performance and a 7.41 final performance, which are enhanced by 178% and 15.8% compared with the optimization performance of the SAGA method in Room 2.

In both scenarios, the LMWO framework effectively harnesses the initialization capabilities of LLMs and continuously optimizes the output with outstanding wireless network planning capacity and the architecture daylight planning capacity, coupled with a rapid exploration speed. Moreover, the results clearly illustrate a substantial optimization potential for window design to improve the overall indoor QoE compared with the UWD strategy. To our best knowledge, three main factors contribute to the powerful optimization capacity of the LMWO framework. Firstly, the pre-trained wireless and architect knowledge embedded in the LLM enables the LMWO framework with a solid initial capacity in a zero-shot fashion. Secondly, the LMWO framework efficiently extracts relevant information from our designed prompts, empowered by the semantic understanding capacity of LLMs, leading to progressively improved solutions. Finally, the human-like continuous learning ability of the LLM leverages external multi-modal feedback from the evaluation system to further enhance the optimization performance.

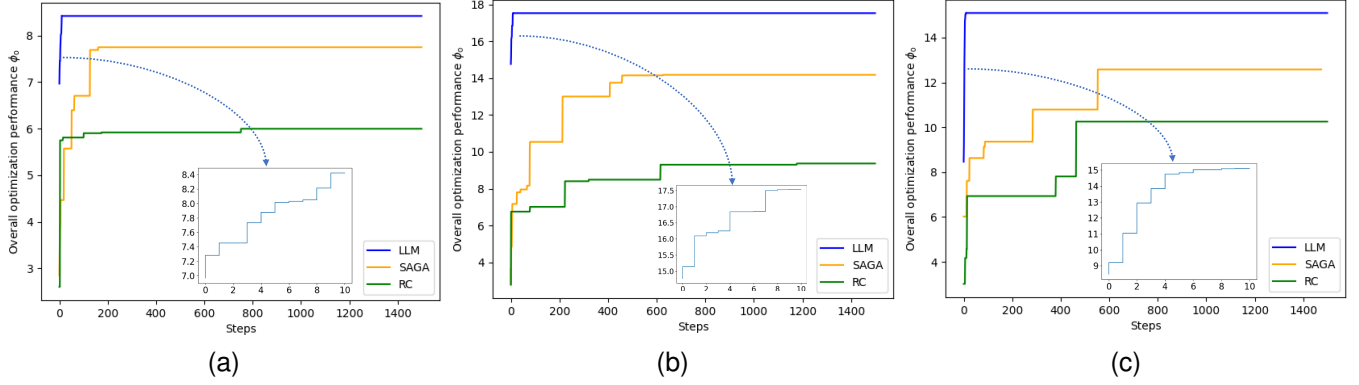


Fig. 6. The average optimization performance of the LMWO framework compared with benchmark methods versus iteration steps in Room 1 with (a) two windows, (b) three windows, and (c) four windows.

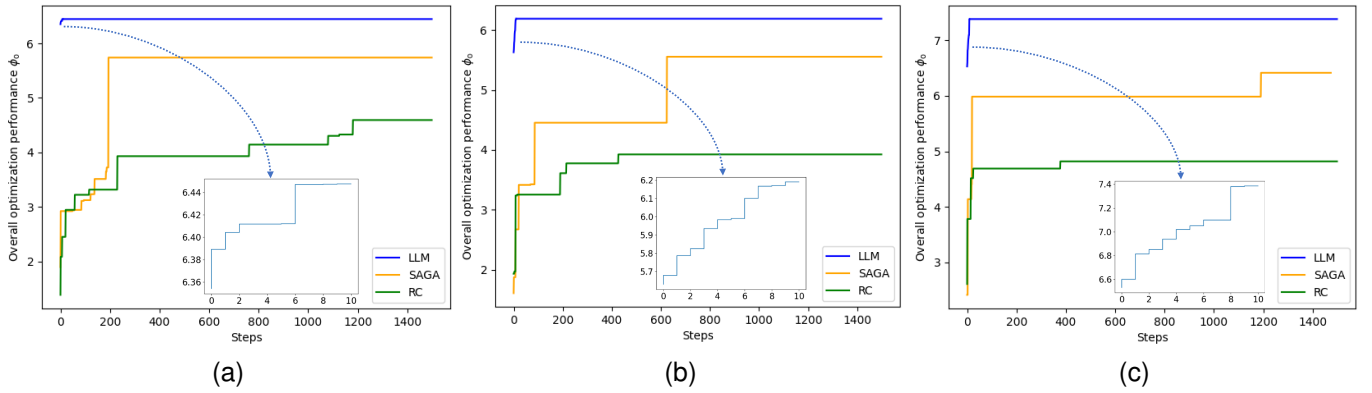


Fig. 7. The average optimization performance of the LMWO framework compared with benchmark methods versus iteration steps in Room 2 with (a) two windows, (b) three windows, and (c) four windows.

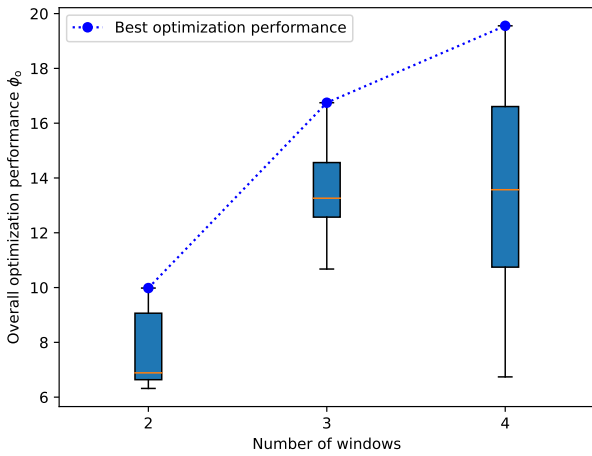


Fig. 8. The reliability and the best optimization performance of the LMWO framework versus the number of windows in Room 1.

C. The Influence of Windows Number

In this subsection, we investigate the influence of the number of windows on the performance and the reliability of the LMWO framework by considering two, three, and four windows. Firstly, Fig. 8 illustrates the influence of the number of windows on the upper bound of optimization performance,

the median value, and the reliability of the LMWO framework in Room 1. As the number of windows increases from 2 to 4, the upper bound of optimization performance rises from 10.1 to around 20. However, the degree of variability in optimization performance also significantly increases. This indicates that more windows can improve the upper bound of optimization, but its reliability is also greatly reduced. This is because an increase in the number of windows leads to a larger solution space and more dispersed RIS units, making the exploration process more challenging. Consequently, while the LMWO framework has a higher optimization ceiling, it becomes more susceptible to local suboptimal solutions, thereby reducing the reliability of the optimization results.

Next, a similar pattern appears in the Room 2 scenario. Fig. 9 illustrates the influence of the number of windows on the performance and the reliability of the LMWO framework by considering two, three, and four windows in Room 2. The optimization upper bound grows from 6.45 to 6.71 and finally reaches around 7.5 as the number of windows increases from two to four. However, the reliability also decreases in this process. This phenomenon further demonstrates that as the solution space becomes larger, the LMWO framework achieves higher optimization extremes but also encounters increased risks of falling into local suboptimal traps.

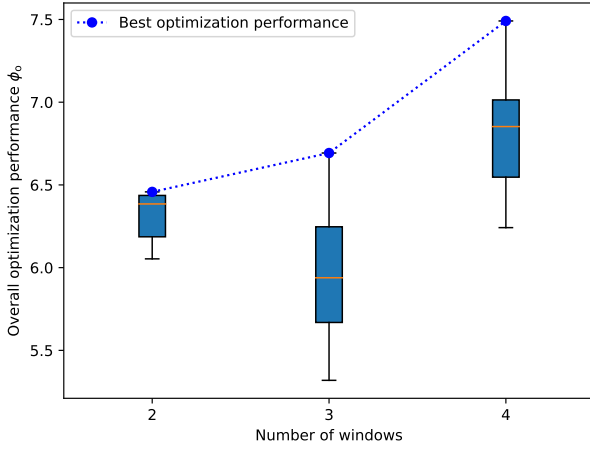


Fig. 9. The reliability and the best optimization performance of the LMWO framework versus the number of windows in Room 2.

D. The Influence of RIS Units Number

We investigate the influence of the number of RIS units on the optimization performance of the LMWO framework. As the number of RIS units increases, the number of RIS units per window also rises. Consequently, the orientations of RISs and the positions of windows play an increasingly critical role in the optimization process. In other words, a higher number of RIS units enhances the optimization tendency toward wireless performance improvement.

Specifically, Fig. 10 demonstrates the influence of the number of RIS units on the average optimization performance of the LMWO framework in Room 1, considering 500, 700, 900, 1100, and 1300 units with two, three, and four windows. In all these scenarios, the average optimization performance exhibits a slightly increasing trend as the number of RIS units increases. Only when the number of RIS units increases from 1100 to 1300, a notable optimization performance is observed with an improvement of 13%. In Room 1, increasing the number of RIS units and enhancing wireless network optimization has a more pronounced effect on the overall optimization performance than the impact on daylight performance. However, the slight improvement ratio indicates that increasing the total number of RIS units to improve the overall optimization performance is limited cost-effectiveness for overall optimization in Room 1. Moreover, when there are three or four windows, the performance of the LMWO framework is very close and exceeds that of the two-window scenario. It demonstrates that a more uniformly distributed RIS unit setup has greater potential for wireless optimization and is more likely to yield effective performance optimization solutions.

An opposite trend is observed in Room 2. Fig. 11 demonstrates the influence of the total number of RIS units on the average performance of the LMWO framework in Room 2, considering 500, 700, 900, 1100, and 1300 units with two, three, and four windows. Overall, the average optimization performance of the LMWO framework decreases with the increase in the number of RIS units. The performance in the two-window scenario is close to, but slightly higher than that

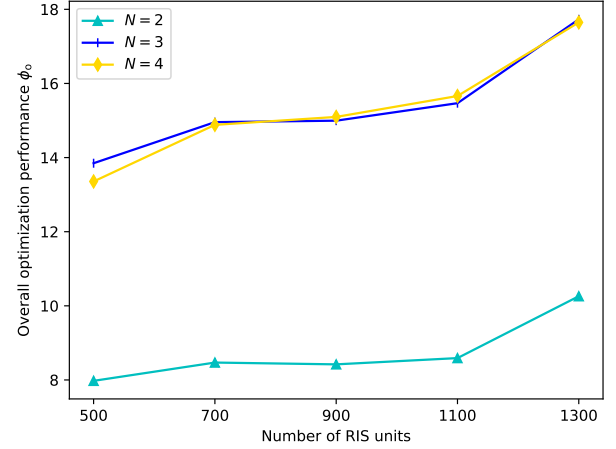


Fig. 10. The average performance improvement achieved by the LMWO framework versus the total units of RISs in Room 1.

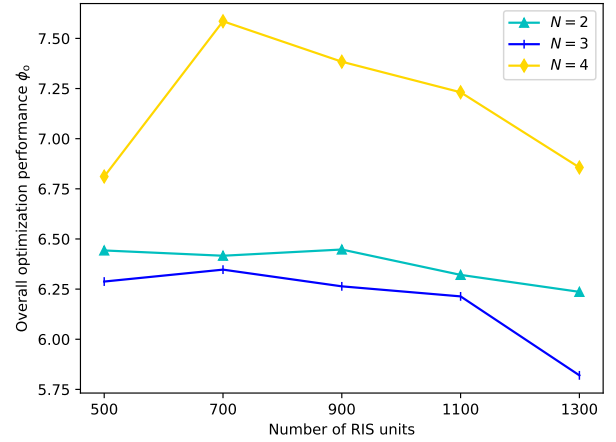


Fig. 11. The average performance improvement achieved by the LMWO framework versus the total units of RISs in Room 2.

in the three-window scenario, which is in turn lower than the performance in the four-window scenario. It demonstrates that as the number of RIS units and the wireless optimization tendency increase, the improvement of wireless performance remains less significant compared to its impact on daylight performance. In addition, a notable phenomenon is that with four windows, the optimization performance of the LMWO framework dramatically increases from 6.78 to more than 7.6 when the number of RIS units increases from 500 to 700. This demonstrates that, with four windows, a more dispersed RIS configuration can yield wireless performance improvements that surpass the impact on daylight performance.

To explain these results, we summarize that the number of windows and the window deployment range create a joint effect on the influence of the number of RIS units on the performance of the LMWO framework. Specifically, the number of windows determines the dispersion degree of RIS units and the deployment range of windows affects the flexibility degrees of both windows and RIS units' deployment. With more windows and a larger window deployment range, an increase in the number of RIS units and a higher tendency for wireless optimization result in greater improvements in

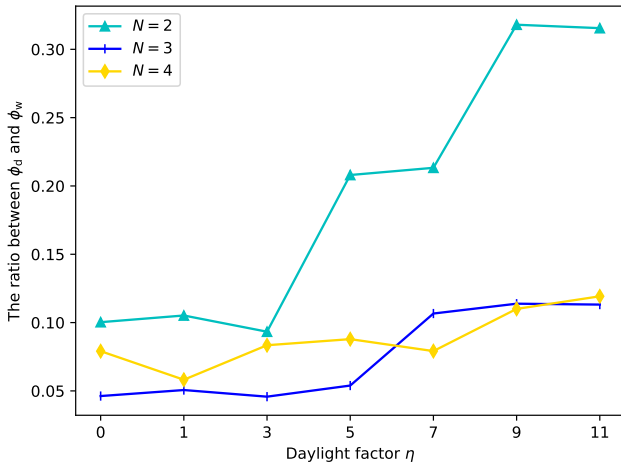


Fig. 12. The ratio between the daylight performance improvement and wireless performance improvement achieved by the LMWO framework versus the daylight factor in Room 1.

wireless performance compared to their impact on daylight performance. In contrast, with fewer windows and smaller deployment ranges, more RIS units and higher wireless optimization tendency not only fail to enhance overall performance but may also lead to a decline.

E. The Influence of Daylight Factor

Furthermore, we investigate the influence of the daylight factor η on the daylight optimization tendency of the LMWO framework, quantified by the ratio of daylight performance improvement ϕ_d^x to wireless performance improvement ϕ_w^x . The daylight factor varies from zero to eleven in increments of two. Specifically, Fig. 12 demonstrates the influence of the daylight factor on the daylight optimization tendency when there are two, three, and four windows in Room 1. We notice that as the daylight factor η increases, the daylight optimization tendency significantly increases across all scenarios. When there are two windows, the daylight optimization tendency remains around 0.1 from daylight factors 0 to 3, followed by a dramatic increase from daylight factor 3 to 11. Moreover, with three and four windows, the daylight optimization tendency gradually increases from 0.05 to 0.1 as the daylight factor increases. This demonstrates that the LMWO method effectively considers the daylight factor, exhibiting a clear daylight optimization tendency and semantic understanding capacity. Moreover, the LMWO framework is more sensitive to the daylight factor when there are fewer windows. This is because fewer windows offer more flexibility in adjusting their positions on the wall, enabling the LMWO framework to more easily identify optimal solutions for enhancing daylight performance.

Similar phenomena are observed in Room 2. Fig. 13 demonstrates the influence of the daylight factor on the daylight optimization tendency in Room 2, considering scenarios with two, three, and four windows. We observe that in scenarios with two and three windows, the daylight optimization tendency remains steady initially but increases rapidly from the daylight factor 3. In contrast, in the four-window scenario, the daylight optimization tendency increases gradually from

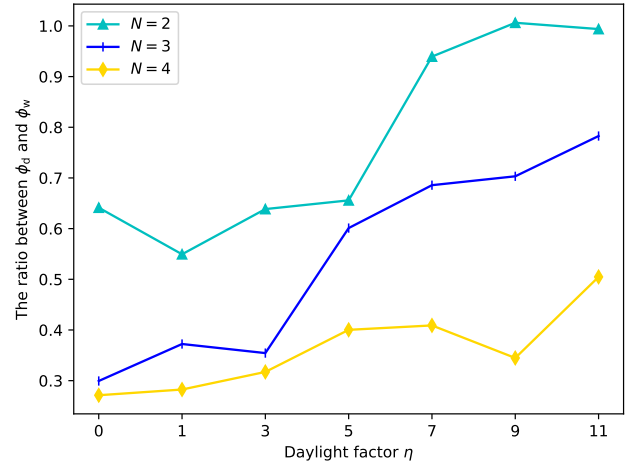


Fig. 13. The ratio between the daylight performance improvement and wireless performance improvement achieved by the LMWO framework versus the daylight factor in Room 2.

TABLE II
AVERAGE OPERATION TIME COSTS

Scenarios	Methods	$N = 2$	$N = 3$	$N = 4$
Room 1	LMWO	33.3 s	36.7 s	41.2 s
	SAGA	2136.17 s	2421.76 s	2962.42 s
	RC	2131.49 s	2416.47 s	2956.49 s
Room 2	LMWO	24.2 s	26.0 s	27.5 s
	SAGA	621.48 s	931.72 s	997.25 s
	RC	616.46 s	926.49 s	991.44 s

0.28 to around 0.5 as the daylight factor increases from 0 to 11. This trend demonstrates that the LMWO framework effectively incorporates the daylight factor, demonstrating both an understanding capacity and a stronger daylight optimization tendency. Moreover, a comparison between Figs. 12 and 13 reveals that smaller rooms offer greater flexibility regarding the daylight factor. This is because, with the same number of windows, smaller rooms allow the LMWO framework and LLMs to more easily propose solutions that enhance daylight performance and focus more on daylight-related improvements.

F. Time Complexity

Eventually, we examine the time complexity of each method including the iterative environmental interaction process across scenarios as shown in Table II. Although the LMWO framework incurs a relatively higher online time cost compared to the RC and SAGA methods due to the internet speed and the sequence generation speed of LLMs, its superior reasoning efficiency still provides significant time advantages. Fig. 14 and Fig. 15 depict the time complexity of optimization methods including the online operation process and interaction process with environments in Room 1 and Room 2, respectively. Comparing these two figures, we observe that time complexity increases as the number of windows and the room size increase. In both scenarios, the LMWO framework exhibits huge advances over the other methods. This is because the LMWO framework only requires fewer than ten iterations to

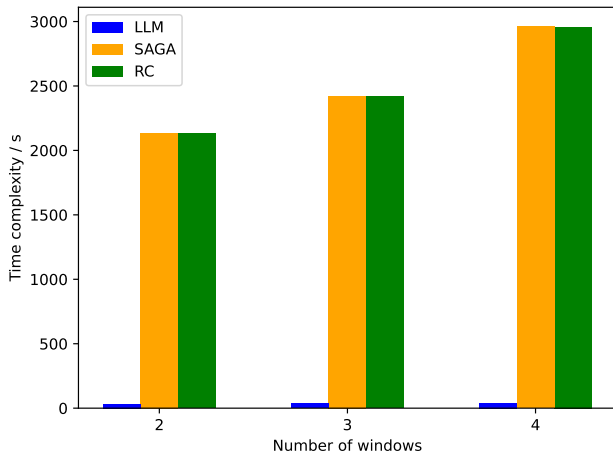


Fig. 14. The time complexity of optimization methods including environmental interaction process in Room 1.

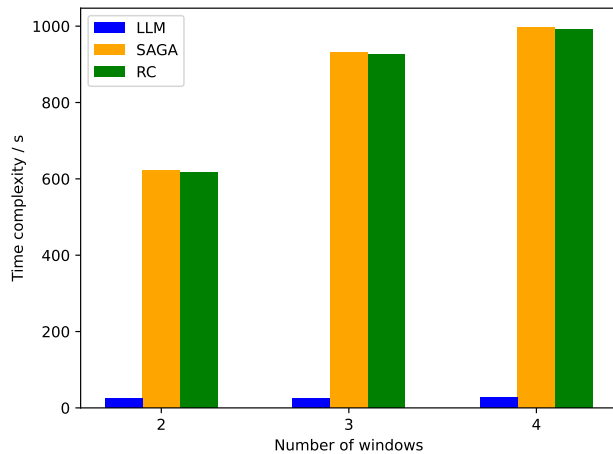


Fig. 15. The time complexity of optimization methods including environmental interaction process in Room 2.

achieve satisfactory stable results benefiting from its pre-train knowledge and fast learning capacity from feedback, instead of hundreds of iterations in the SAGA and RC methods.

VI. CONCLUSION

This paper has addressed a joint optimization of indoor wireless and daylight performance in RIS-aided O2I scenarios. We have highlighted the significance of the window-deployment strategy of T-RIS and formulated an optimization problem that simultaneously considers the wireless and daylight performance. Moreover, a novel optimization framework named LMWO has been proposed to tackle this problem based on the multi-modal LLM technology using prompt engineering technology. Our numerical results have revealed that our proposed LMWO framework significantly improves the overall performance of both wireless and daylight, illustrating the critical role of window placement compared to the uniform distribution strategy. Furthermore, the LMWO framework has shown substantial optimization performance in warm start, exploration speed, and final performance, compared with the SAGA heuristic optimization algorithm. In addition, we have

analyzed the impact of the number of windows, number of RIS units, room size, and daylight factor on the performance of the LMWO framework showcasing its advanced optimization capabilities and the strong generalization ability of our proposed framework. These findings have underscored the significance of window positioning and the potential of LLMs as optimizers in RIS-aided O2I wireless communications scenarios.

REFERENCES

- [1] J. Zhang, A. A. Glazunov, W. Yang, and J. Zhang, "Fundamental wireless performance of a building," *IEEE Wirel. Commun.*, vol. 29, no. 1, pp. 186–193, Feb. 2022.
- [2] J. Y. Dai *et al.*, "Wireless communication based on information metasurfaces," *IEEE Trans. Microw. Theory Tech.*, vol. 69, no. 3, pp. 1493–1510, Mar. 2021.
- [3] H. Zhang *et al.*, "mmWave indoor channel measurement campaign for 5G new radio indoor broadcasting," *IEEE Trans. Broadcast.*, vol. 68, no. 2, pp. 331–344, Jun. 2022.
- [4] M. Nemati, B. Maham, S. R. Pokhrel, and J. Choi, "Modeling RIS empowered outdoor-to-indoor communication in mmWave cellular networks," *IEEE Trans. Commun.*, vol. 69, no. 11, pp. 7837–7850, Nov. 2021.
- [5] R. Liang, J. Fan, H. Liu, Y. Ge, and J. Zhang, "Dual-hop hybrid IRS-aided outdoor-to-indoor mmWave communications," *IEEE Commun. Lett.*, vol. 26, no. 12, pp. 2979–2983, Dec. 2022.
- [6] P. S. Aung, L. X. Nguyen, Y. K. Tun, Z. Han, and C. S. Hong, "Deep reinforcement learning based spectral efficiency maximization in STAR-RIS-assisted indoor outdoor communication," in *NOMS 2023-2023 IEEE/IFIP Network Operations and Management Symposium*. IEEE, Mar. 2023, pp. 1–6.
- [7] J. He, A. Fakhreddine, and G. C. Alexandropoulos, "STAR-RIS-enabled simultaneous indoor and outdoor 3D localisation: Theoretical analysis and algorithmic design," *IET Signal Process.*, vol. 17, no. 4, pp. 1–11, Mar. 2023.
- [8] G.-H. Li, D.-W. Yue, S.-N. Jin, and Q. Hu, "Hybrid double-RIS and DF-relay for outdoor-to-indoor communication," *IEEE access*, vol. 10, no. 3, pp. 126 651–126 663, Dec. 2022.
- [9] Y. Zhou, Y. Shao, J. Zhang, and J. Zhang, "Wireless performance evaluation of building materials integrated with antenna arrays," *IEEE Commun. Lett.*, vol. 26, no. 4, pp. 942–946, Apr. 2022.
- [10] X. Li, "Illegal gym construction leaves 240 families homeless in Harbin," 2023, <https://www.sixthtone.com/news/1012826>, last accessed on 2023-07-23.
- [11] D. Kitayama, Y. Hama, K. Goto, K. Miyachi, T. Motegi, and O. Kagaya, "Transparent dynamic metasurface for a visually unaffected reconfigurable intelligent surface: Controlling transmission/reflection and making a window into an RF lens," *Opt. Express*, vol. 29, no. 18, pp. 29 292–29 307, Aug. 2021.
- [12] X. Xie, C. He, X. Ma, F. Gao, Z. Han, and Z. Jane Wang, "Joint precoding for active intelligent transmitting surface empowered outdoor-to-indoor communication in mmWave cellular networks," *IEEE Trans. Wirel. Commun.*, vol. 22, no. 10, pp. 7072–7086, Oct. 2023.
- [13] B. Liu, Q. Wang, and S. Pollin, "TAIS: Transparent amplifying intelligent surface for indoor-to-outdoor mmWave communications," *IEEE Trans. Commun.*, vol. 72, no. 2, pp. 1223–1238, Apr. 2024.
- [14] M. K. Carroll, A. M. Anderson, S. T. Mangu, Z. Hajjaj, and M. Capron, "Aesthetic aerogel window design for sustainable buildings," *Sustainability (Basel, Switzerland)*, vol. 14, no. 5, p. 2887, Mar. 2022.
- [15] A. Jacobs, Low Energy Architecture Research Unit, LEARN, and London Metropolitan University, "Synthlight handbook, chapter 1: Fundamentals," *European Commission*, pp. 1–46, 2004.
- [16] Z. Li, H. Hu, J. Zhang, and J. Zhang, "Coverage analysis of multiple transmissive RIS-aided outdoor-to-indoor mmWave networks," *IEEE Trans. Broadcast.*, vol. 68, no. 4, pp. 935–942, Dec. 2022.
- [17] Y. Zhang, S. R. Khosravirad, X. Chu, and M. A. Uusitalo, "On the IRS deployment in smart factories considering blockage effects: Collocated or distributed?" *IEEE Trans. Wirel. Commun.*, vol. 23, no. 9, pp. 12 084–12 098, Sep. 2024.
- [18] W. Tang *et al.*, "Path loss modeling and measurements for reconfigurable intelligent surfaces in the millimeter-wave frequency band," *IEEE Trans. Commun.*, vol. 70, no. 9, pp. 6259–6276, Sep. 2022.
- [19] "Grasshopper 3D model software," <https://simplyrhino.co.uk/3d-modelling-software/grasshopper>.

- [20] "The theory of Radiance based on Daysim," <https://www.radiance-online.org/archived/radsite/radiance/refer/long.html>.
- [21] "Indoor environmental input parameters for design and assessment of energy performance of buildings addressing indoor air quality, thermal environment, lighting and acoustics," *European Standard*, pp. 1–49, 2006.
- [22] "Energy power map of Ladybug," <https://www.ladybug.tools/epwmap/>.
- [23] X. Wu, W. Sheng-hao, J. Wu, F. Liang, and K. C. Tan, "Evolutionary computation in the era of large language model: Survey and roadmap," *arXiv: 2401.10034*, pp. 1–19, Feb. 2024.
- [24] T. Teubner and C. M. Flath and C. Weinhardt and W. van der Aalst, and O. Hinz, "Welcome to the era of ChatGPT et al: The prospects of large language models," *Bus. Inf. Syst. Eng.*, vol. 65, no. 2, pp. 95–101, Mar. 2023.
- [25] M. Burtsev, M. Reeves, and A. Job, "The working limitations of large language models," *MIT Sloan Manage. Rev.*, vol. 65, no. 2, pp. 8–10, Nov. 2024.
- [26] Q. Guo *et al.*, "Connecting large language models with evolutionary algorithms yields powerful prompt optimizers," *arXiv: 2309.08532*, pp. 1–24, Feb. 2024.
- [27] "The Ranplan software," <https://www.ranplanwireless.com/gb/>.
- [28] F. Liu, X. Tong, M. Yuan, and Q. Zhang, "Algorithm evolution using large language model," *arXiv:2311.15249*, pp. 1–11, Nov. 2023.
- [29] S. Liu, C. Chen, X. Qu, K. Tang, and Y. Ong, "Large language models as evolutionary optimizers," *arXiv: 2310.19046*, pp. 1–8, Apr. 2023.
- [30] A. J. Thirunavukarasu, D. S. J. Ting, K. Elangovan, L. Gutierrez, T. F. Tan, and D. S. W. Ting, "Large language models in medicine," *Nat. Med.*, vol. 29, no. 8, pp. 1930–1940, Jun. 2023.
- [31] T. Liu, N. Astorga, N. Seedat, and M. van der Schaar, "Large language models to enhance Bayesian optimization," *arXiv: 2402.03921*, pp. 1–33, Mar. 2024.
- [32] J. Shao *et al.*, "WirelessLLM: Empowering large language models towards wireless intelligence," *J. Commun. Inf. Netw.*, vol. 9, no. 2, pp. 99–112, Jun. 2024.
- [33] H. Zhang, A. B. Sediq, A. Afana, and M. Erol-Kantarci, "Large language models in wireless application design: In-context learning-enhanced automatic network intrusion detection," *arxiv.2405.11002*, May 2024.
- [34] D. Krstic, S. Suljovic, G. Djordjevic, N. Petrovic, and D. Milic, "MDE and LLM synergy for network experimentation: Case analysis of wireless system performance in Beaulieu-Xie fading and k- μ co-channel interference environment with diversity combining," *Sensors (Basel, Switzerland)*, vol. 24, no. 10, p. 3037, May 2024.
- [35] Y. Shen *et al.*, "Large language models empowered autonomous edge AI for connected intelligence," *arxiv.2307.02779*, May 2023.
- [36] K. Qiu, S. Bakirtzis, I. Wassell, H. Song, J. Zhang, and K. Wang, "Large language model-based wireless network design," *IEEE Wirel. Commun. Lett.*, p. 1–6, Sep. 2024.
- [37] Q. Liu, J. Mu, D. ChenZhang, Y. Liu, and T. Hong, "LLM enhanced reconfigurable intelligent surface for energy-efficient and reliable 6G IoV," *IEEE Trans. Veh. Technol.*, vol. 24, no. 10, pp. 1–9, May 2024.
- [38] S. Soman and H. G. Ranjani, "Observations on LLMs for telecom domain: Capabilities and limitations," *arxiv.2305.13102*, May 2023.
- [39] H. Zhou, M. Erol-Kantarci, Y. Liu, and H. V. Poor, "A survey on model-based, heuristic, and machine learning optimization approaches in RIS-aided wireless networks," *IEEE Commun. Surv. Tutor.*, pp. 781–823, May. 2023.
- [40] S. Xu, C. K. Thomas, O. Hashash, N. Muralidhar, W. Saad, and N. Ramakrishnan, "Large multi-modal models (LMMs) as universal foundation models for AI-native wireless systems," *arxiv.2402.01748*, Feb. 2024.
- [41] S. Lan and W. Lin, "Genetic algorithm optimization research based on simulated annealing," in *17th IEEE/ACIS International Conference on Software Engineering, Artificial Intelligence, Networking and Parallel/Distributed Computing (SNPD)*, Shanghai, China, Jun. 2016, pp. 491–494.
- [42] R. Haupt and S. Haupt, *Practical Genetic Algorithms*. John Wiley and Sons, 2004.
- [43] "The Anthropic API," <https://www.anthropic.com/api>.